IRSTI 29.17.19 https://doi.org/10.26577/ijmph.20211326

NUMERICAL STUDY OF THE INFLUENCE OF INJECTION MODES ON THE STRUCTURE OF TURBULENT FLAME OF LIQUID HYDROCARBONS IN THE CYLINDRICAL COMBUSTION CHAMBER

S.A. Bolegenova, A.S. Askarova, S.A. Bolegenova, I.E. Berezovskaya*, V.Yu. Maximov, M.Zh. Ryspayeva, A.O. Nugymanova, A.Z. Nurmukhanova, A.A. Kuramay and A.Zh. Balmaganbet

Al-Farabi Kazakh National University, Almaty, Kazakhstan

Email: Yryna.Berezovskaya@kaznu.edu.kz

(Received 1 November 2026; revised 17 November 2026; accepted 18 November 2026)

Abstract. The influence of initial injection velocity on turbulent spray combustion of n-dodecane ($C_{12}H_{26}$) and n-octane (C_8H_{18}) in a model cylindrical chamber was investigated numerically. An Eulerian–Lagrangian approach was used to describe the compressible gas phase and dispersed fuel droplets. The gas-phase conservation equations were coupled with the standard k–ε turbulence model, while droplet breakup and evaporation were described using the Taylor Analogy Breakup model and a diffusion-controlled evaporation model. Injection velocities ranged from 80 to 300 m/s. For n-dodecane, the reported maximum gas temperature was 2200 K at 80 and 100 m/s and 2400 K at all sampled velocities from 150 to 300 m/s. For n-octane, the maximum temperature remained at 2400 K across the sampled velocities at the reported precision. The maximum CO_2 mass fraction was 0.150 for both fuels. The maximum H_2O mass fraction increased from 0.065 to 0.070 for n-dodecane and remained at 0.070 for n-octane. Thus, 150 m/s was the lowest sampled injection velocity at which the reported temperature maxima of the two fuels coincided. The results characterize the sensitivity of local temperature and product mass-fraction maxima to injection velocity and provide a basis for selecting operating conditions for further model validation.

Keywords: spray combustion, numerical modeling, injection velocity, n-dodecane, n-octane.

INTRODUCTION

Under the conditions of the modern global energy transition and the increasingly stringent international environmental regulations, such as Euro-6/7 standards and the International Civil Aviation Organization (ICAO) recommendations for reducing aviation emissions, a key challenge in engineering physics and power engineering is to improve the efficiency of organic fuel combustion while minimizing harmful emissions. Despite the rapid electrification of transport and the development of alternative energy sources, the high-energy-density combustion of liquid hydrocarbon fuels is expected to remain an essential energy source for several decades to come in aviation, heavy marine transport, thermal power generation and heavy-duty machinery [1]. Limitations on the specific capacity of batteries and the weight of equipment make it impossible to completely replace internal combustion engines (ICEs) and gas turbine units (GTU) in the near future, which makes research into optimizing their operating processes extremely relevant [2].

The combustion of liquid fuels in real technological devices is an extremely complex multiphase physical and chemical process. It combines high-intensity hydrodynamics of turbulent flows, primary atomization of a liquid jet discharged from a nozzle, secondary aerodynamic fragmentation of droplets, their stochastic interaction, interphase heat and mass transfer, evaporation into a heated environment, mixing of vapors with an oxidizer and multi-stage chemical kinetics of exothermic oxidation of hydrocarbons [3]. The interactions of velocity fluctuations with the chemical reaction generates pronounces spatial and temporal heterogeneity and non-stationarity, leading to local flame extinctions, pressure pulsations and thermal degradation of the structural

 © 2026 Al-Farabi Kazakh National University

elements of the combustion chamber. For example, the authors of studies [4, 5, 6], as well as other authors of works [7, 8] have examined the influence of the initial parameters of liquid fuel droplets in the combustion chamber on the development of spraying, ignition and combustion, the temperature field, the nature of the flow and the distribution of combustion products.

Experimental study of turbulent combustion at elevated pressure requires measurement of temperature and gas composition with sufficient spatial resolution. For such measurements, noncontact laser methods are used, which require optical access to the area under study. For example, when studying the interaction of a turbulent methane-air flame with a wall, coherent anti-Stokes Raman spectroscopy was combined with laser-induced fluorescence to locally determine the gas temperature and mole fractions of CO_2 and CO. The measurements were carried out on a laboratory setup at atmospheric pressure and at an absolute pressure of 3 bar [9]. Moreover, it is extremely difficult to obtain a comprehensive three-dimensional picture of the distribution of local velocities, microscale vortices and concentration of all reactants and combustion products in the entire volume of the combustion chamber experimentally.

Experimental measurements are supplemented by computational fluid dynamics (CFD) calculations, which allow for the analysis of spatial distributions of velocity, temperature and mass fractions of chemical components in the combustion chamber. Thus, when modeling the turbulent combustion of atomized aviation kerosene using the large eddy simulation (LES) method, the influence of the choice of the chemical kinetics mechanism on the flame structure, temperature and composition of combustion products was investigated [10]. CFD methods are also used to study the combustion of solid fuels. In particular, in calculations of pulverized coal furnaces at thermal power plants in Kazakhstan, they were used to analyze aerodynamics, heat and mass transfer, and the spatial distribution of combustion products [11, 12, 13].

In numerical studies of turbulent combustion, direct numerical simulation (DNS), large eddy simulation (LES) and calculations based on the Reynolds-averaged Navier–Stokes equations (RANS) are used. In the unsteady (URANS) approach, the time evolution of the mean flow is calculated. DNS data are used, in particular, to test turbulent combustion models used in RANS and LES [14].

DNS must resolve small-scale flow structures and subtle zones of chemical reactions. This places high demands on spatial and temporal resolution and limits the application of DNS in series of calculations of full-size combustion chambers [15]. In LES, large flow structures are resolved numerically, and the influence of motions on scales smaller than the filter width is taken into account by a subgrid model. An example of the application of LES to the modeling of combustion of atomized liquid fuel is given in the work [10].

For parametric studies of injection, RANS-based models are used in combination with submodels of droplet decay and evaporation. Thus, in three-dimensional calculations of a diesel engine with the RNG turbulence model, the influence of the injection start moment and the angle between the axes of the fuel jets on the combustion characteristics and emissions was investigated [16].

For fundamental and applied simulations, model component or surrogate components are used instead of multicomponent fuels such as diesel or gasoline, which have variable chemical compositions. N-dodecane ($C_{12}H_{26}$), a long-chain saturated hydrocarbon with a high boiling point and stable thermodynamic properties, has become widely used as a reference model diesel and aviation fuel. To simulate gasoline fractions, n-octane (C_8H_{18}) and its isomers, characterized by higher volatility and lower molecular weight, are traditionally used.

The aim of this work is a numerical study of the influence of kinematic injection parameters (in the speed range from 80 to 300 m/s) on the dynamics of spraying, evaporation, mixture formation and the characteristics of turbulent combustion of n-dodecane and n-octane in a cylindrical

model combustion chamber. The scientific novelty of the study lies in the fact that new and organized data were obtained on how isotherms are distributed in space and change over time, as well as the characteristics of the concentration fields of fuel, water vapor and carbon dioxide. Optimal injection modes were identified to ensure maximum heat dissipation.

MATERIALS AND METHODS OF RESEARCH

The mathematical description of the studied multiphase reacting system is based on the an Eulerian–Lagrangian framework. The gas phase (air, hydrocarbon vapors, reaction products) is considered as a continuous compressible medium in Euler coordinates. The liquid phase (dispersed fuel droplets) is described by tracking the motion of a large number of discrete droplets along their Lagrangian trajectories [17]. The basic equations (1)–(14) are presented for a general description of the modeled processes. The mathematical model is interpreted in more detail in [18].

Basic equations of conservation of gas environment

The dynamics of the gas phase is described by the fundamental system of Navier-Stokes equations for a multicomponent reacting medium, supplemented by source terms of interphase interaction:

- Continuity equation (conservation of mass) for the m-th component of a gas mixture:

$$\frac{\partial \rho_m}{\partial t} + \nabla(\rho_m u) = \nabla\left[\rho D \nabla\left(\frac{\rho_m}{\rho}\right)\right] + \dot{\rho}_m^c + \dot{\rho}^s \delta_{m1} \tag{1}$$

where ρ is the total density of the gas mixture (kg/m^3); ρ_m is the partial density of the m-th component; u is the velocity vector of the gas phase (m/s); D is the diffusion coefficient (m^2/s); $\dot{\rho}_m^c$ is a source term, determined by the rate of chemical reactions; $\dot{\rho}^s$ is a macroscopic source of mass due to the evaporation of droplets of a discrete phase; δ_{m1} is the Kronecker symbol, which records the flow of vaporized fuel as the first component of the mixture.

- Equation of conservation of momentum (law of motion of the gas phase):

$$\frac{\partial(\rho u)}{\partial t} + \nabla\cdot(\rho u u) = -p\nabla - \nabla\left(\frac{2}{3}\rho k\right) + \nabla\cdot\sigma + F^s \tag{2}$$

where p is hydrostatic pressure (Pa); σ is viscous stress tensor; k is kinetic energy of turbulence (m^2/s^2); I is unit tensor; F^s is the vector of the interphase dynamic force that determines the aerodynamic drag and the exchange of momentum between the droplets and the gas.

- Equation of conservation of total energy of a mixture:

$$\frac{\partial(\rho I)}{\partial t} + \nabla\cdot(\rho u I) = -p\nabla\cdot u - \nabla\cdot J + \rho\varepsilon + \dot{Q}^c + \dot{Q}^s \tag{3}$$

where I is the specific internal energy of the gas mixture (J/kg); J is the heat flux vector due to thermal conductivity and diffusion; ε is the rate of dissipation of turbulent energy (m^2/s^3); $\dot{Q}^c$ is heat release as a result of exothermic chemical combustion reactions (W/m^3); $\dot{Q}^s$ is the source term of interphase heat exchange, taking into account convective heating and the latent heat of phase transition (evaporation).

To close the system of equations for turbulent characteristics, a two-parameter k–ε turbulence model is used. The equations for the transfer of turbulence kinetic energy k and its dissipation rate ε are written taking into account modifications for phase conjugation:

$$\frac{\partial(\rho k)}{\partial t} + \nabla\cdot(\rho u k) = -\frac{2}{3}\rho k\nabla\cdot u + \sigma : \nabla u + \nabla\cdot\left[\left(\frac{\mu}{\mathrm{Pr}_k}\right)\nabla k\right] - \rho\varepsilon + \dot{W}^s \tag{4}$$

$$\frac{\partial(\rho\varepsilon)}{\partial t}+\nabla\cdot(\rho u\varepsilon)=-\left(\frac{2}{3}C_{\varepsilon1}-C_{\varepsilon3}\right)p\varepsilon\nabla\cdot u - \nabla\cdot\left[\left(\frac{\mu}{\mathrm{Pr}_\varepsilon}\right)\nabla\varepsilon\right] + \frac{\varepsilon}{k}\left[C_{\varepsilon1}\sigma:\nabla u-C_{\varepsilon2}\rho\varepsilon\right] + \dot{W}^{s\varepsilon} \tag{5}$$

where μ is the dynamic viscosity; Pr_k, Pr_ε are the turbulent Prandtl numbers; $C_{\varepsilon1}$, $C_{\varepsilon2}$, $C_{\varepsilon3}$ are the empirical constants of the turbulence model; $\dot{W}^s$, $\dot{W}^{s\varepsilon}$ are additional terms of the interaction of discrete drops with turbulent eddies.

Discrete Phase Modeling. Stochastic Lagrangian Method

The state of an ensemble of injected fuel droplets is described by the probability density function $f(x,v,r,T_d,y,dy/dt,t)$, which depends on the spatial coordinates x, the components of the droplet velocity v, its radius r, temperature T_d and deformation parameters y. The change in the distribution function over time is described by a kinetic equation of the Boltzmann-Vlasov type:

$$\frac{\partial f}{\partial t}+\nabla_x\cdot(fv)+\nabla_v\cdot(fF)+\frac{\partial}{\partial r}(fR) + \frac{\partial}{\partial T_d}\left(f\dot{T}_d\right)+\frac{\partial}{\partial y}\left(f\dot{y}\right)+\frac{\partial}{\partial \dot{y}}\left(f\ddot{y}\right) = \dot{f}_{coll}+\dot{f}_{bu} \tag{6}$$

where F is droplet acceleration under the action of external forces; R is rate of change of droplet radius during evaporation; $\dot{f}_{coll}$, $\dot{f}_{bu}$ are collision integrals describing collisions (coalescence/rebound) and aerodynamic breakup of droplets, respectively.

The equation of motion of an individual drop along its Lagrangian trajectory has the form:

$$\frac{dx}{dt}=v \tag{7}$$

$$\frac{dv}{dt}=F=\frac{3}{8}\frac{\rho}{\rho_l}\frac{\lfloor u+u'-v\rfloor}{r}\left(u+u'-v\right)C_D + g \tag{8}$$

where ρ_l is the density of liquid fuel; g is the gravitational acceleration vector; u' is the pulsating component of gas velocity generated on the basis of an isotropic Gaussian distribution to account for the turbulent transfer of droplets; C_D is the droplet drag coefficient, determined depending on the Reynolds number Re:

$$C_D=\begin{cases}\dfrac{24}{\mathrm{Re}}\left(1+0.15\,\mathrm{Re}^{0.687}\right), & \mathrm{Re}\le 1000,\\ 0.44, & \mathrm{Re}>1000.\end{cases} \tag{9}$$

Models of decomposition, evaporation and chemical kinetics

Hydrodynamic breakup of droplets in a high-speed flow is described by the Taylor Analogy Breakup (TAB) model, based on the analogy between a deforming droplet and a damped spring oscillator. The dimensionless displacement of the drop surface y is described by the equation of harmonic oscillations:

$$\ddot{y}+\frac{5\mu(T_d)}{\rho_l r^2}\dot{y}+\frac{8\sigma}{\rho_l r^3}y=\frac{2}{3}\frac{\rho\lfloor u+u'-v\rfloor^2}{\rho_l r^2} \tag{10}$$

where σ is a coefficient of surface tension of a liquid; $\mu(T_d)$ is a liquid viscosity. The condition for the destruction of a droplet into smaller daughter fragments occurs when critical deformation is reached $y>1.0$. The average radius of the resulting droplets is calculated using Sauter's formula (11) (r_{32}) and is written in the following form:

$$r_{32}=\frac{\int r^3 f\,dr}{\int r^2 f\,dr} \tag{11}$$

The process of phase transition (evaporation) of a liquid droplet is described by a differential equation for the change in its radius:

$$\frac{dr}{dt}=R=-\frac{\rho D}{2\rho_l r}\mathrm{Sh}_d\ln(1+B_M) \tag{12}$$

where Sh_d Sherwood diffusion number; B_M is Spalding's dimensionless mass transport parameter, defined by the expression:

$$B_M=\frac{Y_1^*-Y_1}{1-Y_1^*} \tag{13}$$

where Y_1^* is the equilibrium mass fraction of fuel vapor on the surface of a drop, calculated on the basis of Dalton's law and the saturated vapor pressure $p_v(T_d)$:

$$Y_1^* = \frac{W_0\, p_v(T_d)}{W_0\, p_v(T_d) + W_g\,(p - p_v(T_d))} \qquad (14)$$

where W_0, W_g are molar masses of fuel and surrounding gas, respectively.

Geometrical parameters of the combustion chamber, initial and boundary conditions

The computational domain is a model combustion chamber of cylindrical shape shown in Figure 1 with the following characteristics:

- Chamber height (H): 0.10 m;
- Chamber radius (R): 0.02 m;
- Mesh: 600 structured control volumes.

The following initial conditions were taken into account in the calculations: at the inlet through the injector, the injection of two types of fuel is set with a variable initial velocity v_{in} from 80 to 300 m/s. On the axis $r = 0$ the condition of axial symmetry is set. For two fuels, the mass was 8 mg, the temperature in the combustion chamber at the initial moment was 950 K, the nozzle diameter was 0.005 m. The fuel combustion time was 4 ms. The combustion chamber wall temperature was 353 K. The initial average radius of the injected droplets was 3 micrometers. The chamber pressure was 4 MPa. The nozzle was located in the lower central part of the chamber.

Numerical methods

Numerical modeling of the three-dimensional unsteady reactive multiphase flow with the developed fuel spray was conducted using the KIVA software package. The basic hydrodynamic solver implements the finite volume method on 3D structured grids using the Arbitrary Lagrangian-Eulerian (ALE) scheme.

Chemical-kinetic mechanism: The mathematical model of combustion is divided into two

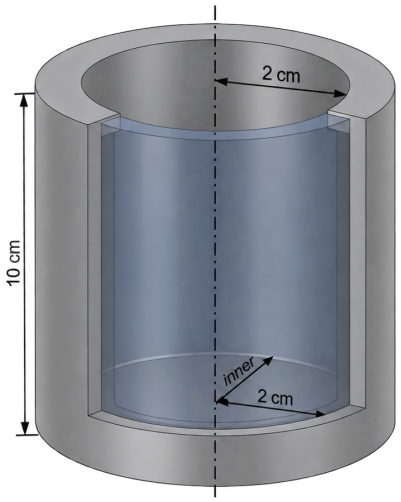


Figure 1 - General view of the combustion chamber

groups of reactions: Kinetic (slow) reactions: kinetic reactions are described by the extended Arrhenius law and integrated using a partial implicit scheme that guarantees non-negativity of the component concentrations at any time steps. Equilibrium (fast) reactions: equilibrium reactions are calculated using the universal iterative solver CHEMEQ.

The main step of the calculation cycle Δt is calculated automatically before each cycle from the accuracy conditions (limitations on local temperature increase from chemical heat generation f_{ch}, spray evaporation rate f_{sp}, relative deformation of cells and maximum step increase $\Delta t^{n+1} \leq 1.02\,\Delta t^n$, since acoustic thermionic and diffusion processes are solved implicitly in phase B).

Convective substep Δt_c: in the phase of explicit grid recalculation and convection (Phase C) the working step is divided into subcycles $\Delta t_c = \Delta t / N_S$, imited by the Courant–Friedrichs–Lewy condition to maintain numerical stability.

Spatial resolution and grid structure: The computational domain is discretized on a three-dimensional hexahedral (Staggered Grid) of size $N_x \times N_y \times N_z$ cells along logical coordinate directions (i, j, k) in the Cartesian coordinate system. Thermodynamic scalar quantities (p, ρ, T, Y_m, I, k, ε) are defined at the cell centers, and the velocity vectors $\bar{u}$ are defined at the vertices. The spatial resolution along the axes Δx, Δy, Δz is de-

termined by the geometric parameters of the combustion chamber.

Setting the fuel mass and injection velocity: The injector characteristics and fuel delivery parameters are specified in the `ITAPE` input data file (`INJECT` subroutine): the `TSPMAS` parameter specifies the total mass of fuel in grams (g) injected during the `TDINJ` pulse duration. At constant injection speed (`PULSE` = 2.0): a fixed value of the jet flow velocity `VELINJ` (cm/s) and the nozzle area are set.

Results and Discussion

The influence of injection modes on the combustion of dodecane

N-dodecane ($C_{12}H_{26}$), being a model component of diesel fuel, is characterized by a relatively high boiling point and density. Numerical experiments have shown that injection kinematics has a decisive influence on the degree of atomization and the intensity of subsequent heat generation.

An analysis of the dependence of the maximum temperature in the combustion chamber on the initial fuel injection velocity revealed a nonlinear nature. In the speed range from 80 m/s to 150 m/s, an intensive increase in the peak temperature in the volume is observed from 2200 K to 2400 K. An increase in the injection velocity contributes to a higher Reynolds number of the jet, intensification of the process of secondary fragmentation of droplets, a decrease in the average radius according to Sauter (r_{32}) and acceleration of the phase transition. As a result, the contact area of the fuel vapor with the oxidizer increases sharply, which ensures a more complete and rapid chemical reaction.

However, with a further increase in injection speed, above 150 m/s to 300 m/s, the maximum temperature remains almost unchanged at 2400 K. This indicates that at $v_{\text{in}} \geq 150$ m/s the limiting stage of the process is not the mixture formation rate, but the chemical kinetics of combustion and the limitation of the presence of oxygen in local zones. Thus, the speed of 150 m/s is the lowest investigated injection velocity at which the maximum temperature for n-dodecane reached 2400 K.

Based on the calculation, the isotherms of the gas phase in the axial section of the combustion chamber (Fig. 2) were analyzed at an injection speed of 150 m/s at different points in time:

- Initial stage ($t = 1.0$ ms): The injected spray of n-dodecane begins to evaporate. The high temperature zone is localized in the lower part of the chamber near the nozzle (height $H \approx 3.8$ cm, radius $R \approx 1.0$ cm). Maximum temperature is about 1400 K.
- Stage of development ($t = 3.2$ ms): Combustion develops further. The hot zone's coverage increases to $H = 5.0$ cm and $R = 1.6$ cm. The maximum temperature rises to 2200 K due to the active exothermic release of heat.
- Final stage ($t = 4.0$ ms): a stable combustion zone has formed, covering the central part of the chamber ($H = 5.8$ cm, $R = 2.0$ cm). Maximum temperature reaches 2400 K. Near the walls, a temperature drop to 1000–1200 K is observed due to convective heat dissipation.

The dynamics of the concentration of fuel vapors ($C_{12}H_{26}$) in Figure 3 demonstrates that at the stage of 1.0 ms the maximum mass fraction of vapors (0.022 g/g) is concentrated at the nozzle. By 3.2 ms, the vapor distribution area increases under the influence of turbulent diffusion. By the time of 4.0 ms, the vapor concentration in the lower part of the nozzle drops, and the zone of maximum concentration shifts upward ($H \approx 3.0$ cm), which indicates complete burnout of the main mass of incoming fuel.

The distribution of combustion products of water vapor (H_2O) and carbon dioxide (CO_2) is shown in Figure 4 and it correlates with the temperature field. The maximum mass fraction of H_2O increases from 0.05 g/g at the initial stage to 0.07 g/g in the developed mode. For CO_2, the maximum relative concentration increases from 0.12 g/g to 0.15 g/g at 4.0 ms. The combustion products are concentrated in the epicenter of the chemical reaction (the middle part of the chamber) and gradually diffuse throughout the volume.

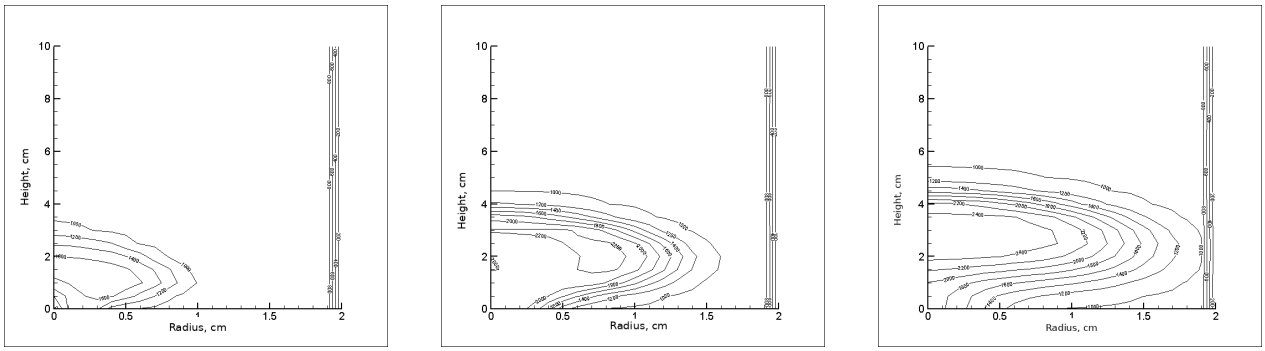


Figure 2 - Isotherms of the gas phase in the axial section of the combustion chamber during injection of n-dodecane at times: a) 1 ms; b) 3.2 ms; c) 4 ms.

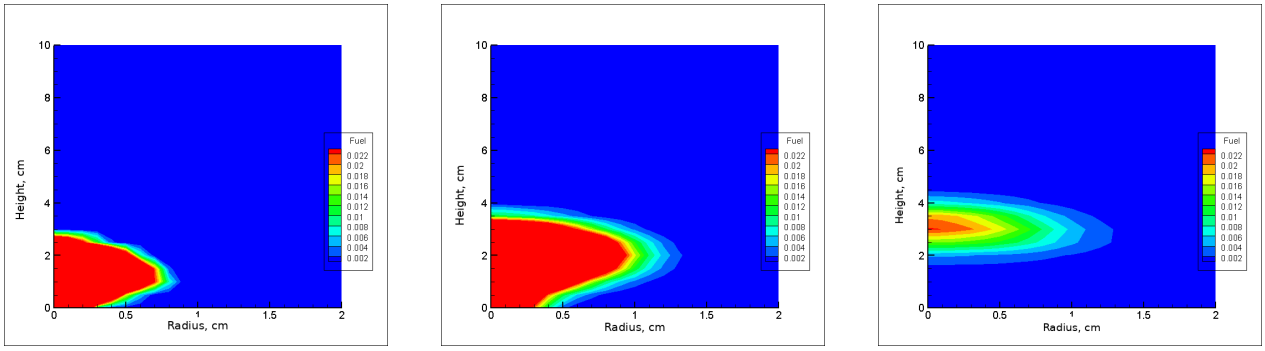


Figure 3 - Graph of distribution of n-dodecane vapors in the combustion chamber at a velocity of 150 m/s at moments of time: a) 1 ms; b) 3.2 ms; c) 4 ms

The influence of injection modes on n-octane combustion

N-octane (C_8H_{18}) is a lighter and more volatile hydrocarbon used as a gasoline fuel substitute.

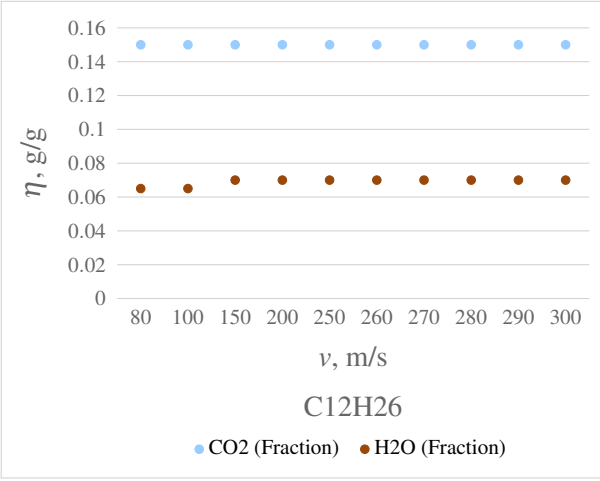


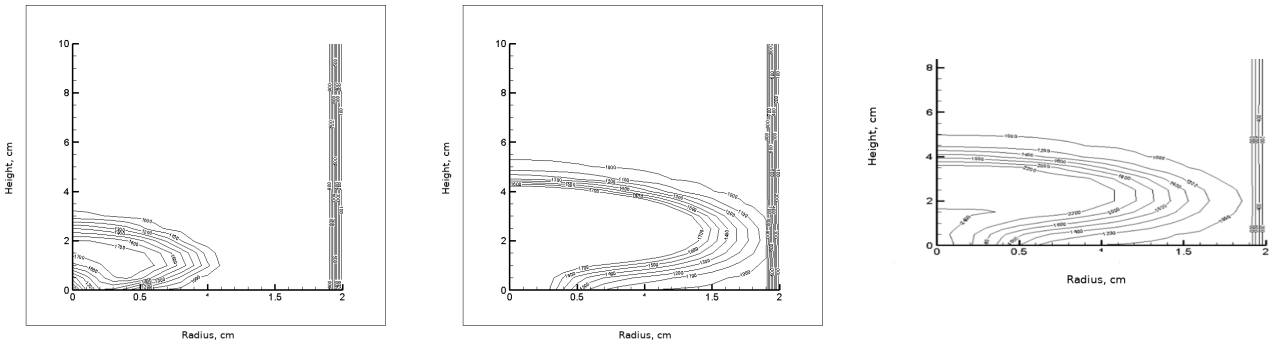
Figure 4 - Maximum mass fractions of CO_2 and H_2O during n-dodecane combustion depending on the initial injection velocity.

The calculations performed showed qualitatively different combustion patterns of octane compared to n-dodecane.

Unlike n-dodecane, the maximum combustion temperature of n-octane turned out to be practically invariant to the injection velocity. The maximum gas temperature remained approximately 2400 K throughout the investigated injection velocity range of 80–300 m/s. This is explained by the high evaporation rates of n-octane, due to which the light fractions have time to completely mix with the oxidizer even at relatively low injection velocities.

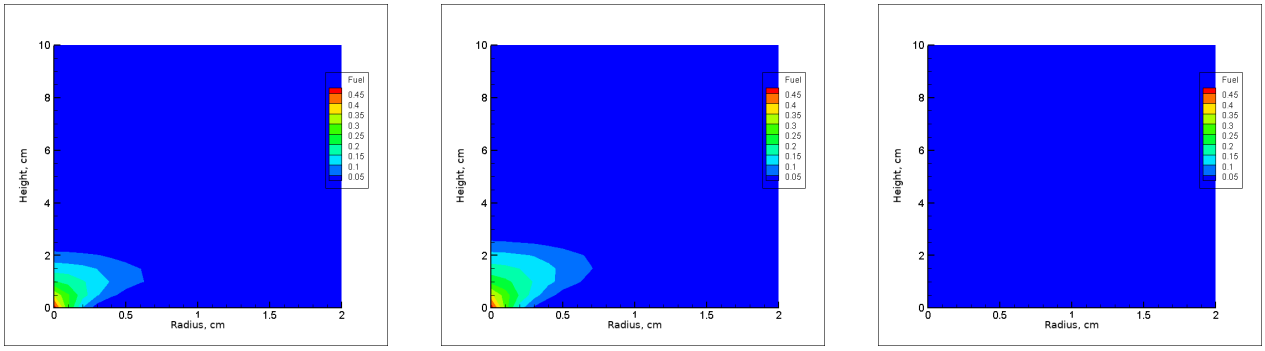
Despite the same temperature maximum, the n-octane injection speed is 150 m/s, since at this speed the most uniform and stable spread of the temperature front is achieved without sharp local gradients.

Figure 5 shows the evolution of the n-octane temperature field at an injection velocity of



a) b) c)

Figure 5 - Isotherms of the gas phase in the axial section of the combustion chamber during n-octane injection at times: a) 1.2 ms; b) 2.7 ms; c) 4 ms.



a) b) c)

Figure 6 - Graph of fuel vapor distribution in the combustion chamber during n-octane injection at a velocity of 150 m/s at times: a) 1.2 ms; b) 2.7 ms; c) 4 ms.

150 m/s and is characterized by the following indicators:

- At the moment of time $t = 1.2$ ms: Autoignition occurs. The flame height is 3.0 cm, its radius is 1.1 cm, temperature $T_{\max} = 1700$ K.
- At the time of combustion $t = 2.7$ ms: The flame expands to $H = 4.0$ cm, $R = 1.5$ cm. A stable elongated shape of flame is formed.
- Final stage of the process $t = 4.0$ ms: The high-temperature field covers a zone of $H = 5.5$ cm and $R = 2.0$ cm. The temperature field reaches 2400 K.

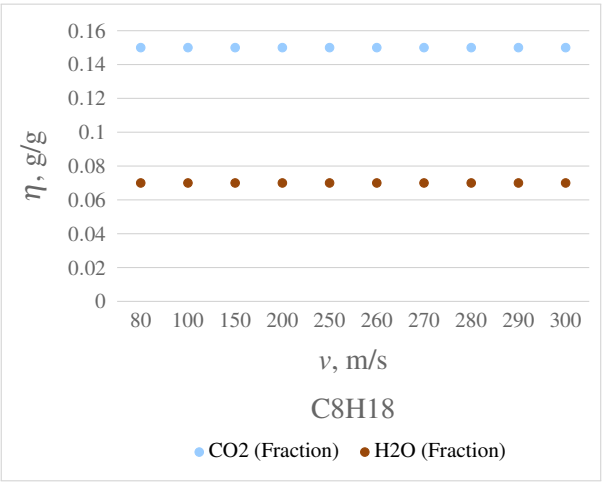


Figure 7 - Dependence of the maximum concentration of reaction products on the injection velocity

A special feature of n-octane is the dynamics of fuel vapors shown in Fig. 6. At the initial stage (1.2 ms), due to high volatility, the mass fraction of vapors at the nozzle reaches a significant value – 0.45 g/g. By 2.7 ms, the concentration decreases to 0.40 g/g. By the time $t = 4.0$ ms, there is no unburned fuel in the chamber volume (the concentration drops to zero), which proves complete combustion of n-octane in the selected mode.

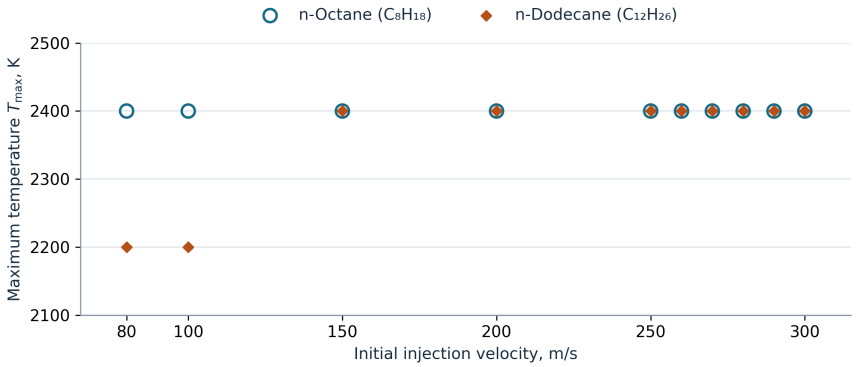
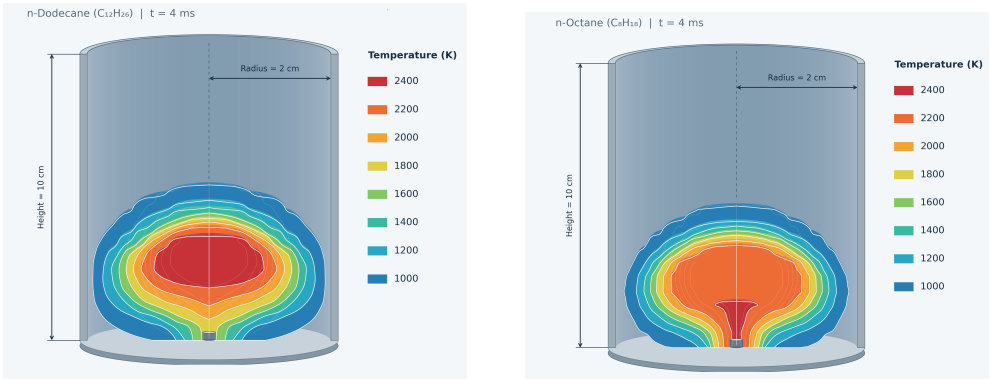


Figure 8 - Dependence of the maximum gas temperature on the initial injection rate of n-octane (C_8H_{18}) and n-dodecane ($C_{12}H_{26}$)



a) b)

Figure 9 - Isosurfaces of gas temperature in a cylindrical combustion chamber at $t = 4$ ms for (a) n-dodecane and (b) n-octane. The isosurfaces were reconstructed by revolving the isotherms from the axial section about the chamber axis.

The dependence of the maximum concentration of reaction products on the injection velocity is shown in Figure 7. The maximum mass fraction of H_2O reaches 0.07 g/g at 4.0 ms and CO_2 reaches 0.15 g/g. The graph demonstrates the thermodynamic stability of the combustion process of n-octane with a change in velocity from 80 to 300 m/s.

Comparative analysis of combustion of n-dodecane and n-octane

A comparative analysis of the obtained results of numerical modeling reveals differences in the combustion physics of heavy (diesel) and light (gasoline) model fuels. Figure 8 shows the dependence of the recorded maximum gas temperature on the initial injection velocity of n-octane and n-dodecane. For n-octane in all presented calculation modes from 80 to 300 m/s, the maximum temperature is 2400 K within the accuracy of the reported data. For n-dodecane it is 2200 K at 80 and 100 m/s and 2400 K at all studied velocities from 150 to 300 m/s. Thus, the greatest difference between the fuels is observed at the two lowest injection velocities and is 200 K.

The weak sensitivity of the maximum temperature to the injection velocity may be attributed to the formation of the hottest regions under similar local combustion conditions. If the fuel-air mixture composition and its enthalpy vary slightly in these regions, changes in the injection velocity may primarily affect the spatial temperature distribution and the flame development dynamics. As shown in Figure 9, the isosurfaces are reconstructed by rotating the axial section isotherms around the chamber axis. At time $t = 4$ ms the

high temperature region for both fuels is concentrated in the lower part of the chamber. For n-dodecane (a), the 2400 K isosurface covers a relatively wide core along the chamber axis, located above the nozzle. The velocity of 150 m/s is the lowest of the studied velocities at which the calculated temperature maximum of n-dodecane reaches 2400 K. For n-octane (b), the 2400 K isosurface is localized near the nozzle, and above it, the hot region expands, which can be seen from the 2200 K isosurface. The difference in the position of the hottest zones is due to differences in the evaporation of droplets and the mixing of fuel vapors with air. More volatile n-octane can form a combustible mixture closer to the injector. For n-dodecane, with slower evaporation of droplets, conditions for the formation of a hot zone can develop further downstream. Isosurfaces show where the gas reaches a given temperature. Thus, the main differences appear in the shape and position of the hottest regions.

Conclusion

Within the Eulerian–Lagrangian model of a multiphase reacting flow, the influence of injection conditions on the structure of a turbulent flame of liquid hydrocarbons in a cylindrical combustion chamber was studied. For n-octane (C_8H_{18}) and n-dodecane ($C_{12}H_{26}$) injection velocities from 80 to 300 m/s were considered, the maximum gas temperatures and mass fractions of CO_2 and H_2O were compared across the simulated injection conditions. For n-octane, the maximum gas temperature was 2400 K at all studied velocities and for n-dodecane, it was 2200 K at 80 and 100 m/s and 2400 K at all velocities from 150 to 300 m/s. Thus, at 80 and 100 m/s, the temperature maximum of n-dodecane was 200 K lower than that of n-octane, and 150 m/s was the lowest of the studied velocities at which the maxima for the two fuels coincided. As shown by the isosurfaces, the main differences are observed in the location of the high-temperature region.

The maximum mass fraction of CO_2 is 0.15 g/g for both fuels in all considered modes. or n-octane, the maximum mass fraction of H_2O is 0.07 g/g, and for n-dodecane it increased from 0.065 g/g at 80 and 100 m/s to 0.07 g/g at the studied velocities from 150 to 300 m/s. The obtained trends indicate that the 100 and 150 m/s injection velocities should be selected for further research, as a change in the maximum temperature of n-dodecane is observed between these two conditions.

Funding

The research received financial support from the Ministry of Science and Higher Education of the Republic of Kazakhstan under grant No. AP26105185.

Author Contributions: S.B.: Supervision; A.A.: Conceptualization; S.B.: Conceptualization, Funding acquisition; I.B.: Data curation, Writing – original draft; V.M.: Writing – review & editing; M.R.: Software, Translation; A.N.: Resources; A.N.: Methodology; A.K.: Draft preparation, Validation; Investigation; A.B.: Draft preparation, Visualization.

References

[1] Pignatelli, F., M. Passad, A. Åkerblom, T. Nilsson, E. J. K. Nilsson, and C. Fureby, "Predictions of spray combustion using conventional category A fuels and exploratory category C fuels." in *AIAA SCITECH 2023 Forum*. American Institute of Aeronautics and Astronautics, 2023, DOI: 10.2514/6.2023-1486.

[2] Varma, A. R., S. Singh, R. Rajasegar, and A. Srna. "Computational analysis of flame initiation, quenching, and re-ignition in a prechamber natural gas engine under varying EGR-dilution levels." *Fuel* 375 (2024): 132529, DOI: 10.1016/j.fuel.2024.132529.

[3] Palies, P. "Flow and flame mechanisms for swirl-stabilized combustors." *Aerospace* 12, no. 5 (2025): 430, DOI: 10.3390/aerospace12050430.

[4] Askarova, A., S. Bolegenova, S. Ospanova, K. Bolegenova, and A. Nurmukhanova. "Energetic efficiency of turbulent biofuel combustion for advanced bioenergy technologies." *International Journal of Mathematics and Physics* 16, no. 1 (2025): 20–28, DOI: 10.26577/ijmph.20251612.

[5] Ryspayeva, M. and I. Berezovskaya. "Numerical simulation of turbulent combustion of liquid fuels: Comparative analysis of benzene and tridecane." *Bulletin of the Karaganda University. Physics Series* 30, no. 4 (120) (2025): 74–82, DOI: 10.31489/2025PH4/74-82.

[6] Berezovskaya, I. E., A. A. Tasmukhanova, M. Z. Ryspaeva, and S. S. Ospanova. "Investigation of the influence of liquid fuel injection rate on the combustion process using KIVA–II software." *Eurasian Physical Technical Journal* 20, no. 3 (45) (2023): 43–51, DOI: 10.31489/2023No3/43-51.

[7] Askarova, A., S. Bolegenova, S. Ospanova, N. Slavinskaya, A. Aldiyarova, and N. Ungarova. "Simulation of non-isothermal liquid sprays under large-scale turbulence." *Physical Sciences and Technology* 8, no. 3-4 (2021): 28–40, DOI: 10.26577/phst.2021.v8.i2.04.

[8] Bolegenova, S., A. Askarova, N. Slavinskaya, S. Ospanova, A. Maxutkhanova, A. Aldiyarova, and D. Yerbosynov. "Statistical modeling of spray formation, combustion, and evaporation of liquid fuel droplets." *Physical Sciences and Technology* 9, no. 3-4 (2022): 69–82, DOI: 10.26577/phst.2022.v9.i2.09.

[9] Johe, P., F. Zentgraf, M. Greifenstein, B. Böhm, and A. Dreizler. "Effects of elevated pressure on thermochemical states of turbulent flame-wall interaction studied by multi-parameter laser diagnostics." *Combustion and Flame* 260 (2024): 113214, DOI: 10.1016/j.combustflame.2023.113214.

[10] Åkerblom, A. and C. Fureby. "LES modeling of the DLR generic single-cup spray combustor: Validation and the impact of combustion chemistry." *Flow, Turbulence and Combustion* 112, no. 2 (2024): 557–585, DOI: 10.1007/s10494-023-00512-4.

[11] Askarova, A., S. Bolegenova, P. Safarik, V. Maximov, and M. Beketayeva. "Heat and mass transfer processes at high-temperature media during combustion of low-grade pulverized coal." *International Journal of Mathematics and Physics* 9, no. 1 (2018): 60–69, DOI: 10.26577/ijmph.2018.v9i1.247.

[12] Askarova, A. S., S. A. Bolegenova, S. A. Bolegenova, V. U. Maximov, A. O. Nugymanova, and P. Safarik. "Combustion processes in furnace chambers of Kazakhstan TPPs using high-ash coal." *International Journal of Mathematics and Physics* 8, no. 2 (2017): 51–60, DOI: 10.26577/ijmph.2017.v8.i2.09.

[13] Bolegenova, S. A., A. S. Askarova, A. Bekmukhamet *et al.* "3D modeling high temperature flows in the combustion chambers of the power plants." *International Journal of Mathematics and Physics* 7, no. 1 (2016): 73–82. https://ijmph.kaznu.kz/index.php/kaznu/article/view/163

[14] Zhou, L. "A review for the progress in validation of the SOM turbulent combustion model by DNS." *International Communications in Heat and Mass Transfer* 159, no. Part B (2024): 108099, DOI: 10.1016/j.icheatmasstransfer.2024.108099.

[15] Domingo, P. and L. Vervisch. "Recent developments in DNS of turbulent combustion." *Proceedings of the Combustion Institute* 39, no. 2 (2023): 2055–2076, DOI: 10.1016/j.proci.2022.06.030.

[16] Cengiz, C. and S. O. Unverdi. "A CFD study on the effects of injection timing and spray inclusion angle on performance and emission characteristics of a DI diesel engine operating in diffusion-controlled and PCCI modes of combustion." *Energies* 16, no. 6 (2023): 2861, DOI: 10.3390/en16062861.

[17] Meng, Q., H. Wang, Z. Huang, K. Luo, and J. Fan. "Direct numerical simulation of ammonia spray combustion ignited by n-heptane flame under high-pressure conditions." *Applications in Energy and Combustion Science* 23 (2025): 100343, DOI: 10.1016/j.jaecs.2025.100343.

[18] Amsden, A. A., P. J. O'Rourke, and T. D. Butler, "KIVA-II: A computer program for chemically reactive flows with sprays." Los Alamos National Laboratory, Los Alamos, NM, Report LA-11560-MS, 1989, DOI: 10.2172/6228444.

Information about authors

S.A. Bolegenova *– PhD, Associate Professor, Al-Farabi Kazakh National University, Almaty, Kazakhstan, e-mail: bolegenova.symbat@kaznu.edu.kz*

A.S. Askarova *– Doctor of Physical and Mathematical Sciences, Professor, Al-Farabi Kazakh National University, Almaty, Kazakhstan, e-mail: aliya.askarova@kaznu.edu.kz*

S.A. Bolegenova *– Doctor of Physical and Mathematical Sciences, Professor, Head of Department, Al-Farabi Kazakh National University, Almaty, Kazakhstan, e-mail: saltanat.bolegenova@kaznu.edu.kz*

I.E. Berezovskaya (corresponding author) *– PhD, Senior Lecturer, Al-Farabi Kazakh National University, Almaty, Kazakhstan, e-mail: Yryna.Berezovskaya@kaznu.edu.kz*

V.Yu. Maximov *– PhD, Professor, Al-Farabi Kazakh National University, Almaty, Kazakhstan, e-mail: valeriy.maximov@kaznu.edu.kz*

M.Zh. Ryspayeva *– PhD, Senior Lecturer, Al-Farabi Kazakh National University, Almaty, Kazakhstan, e-mail: ryspaeva.maiya@gmai.com*

A.O. Nugymanova *– PhD, Associate Professor, Al-Farabi Kazakh National University, Almaty, Kazakhstan, e-mail: aizhan.nugymanova@kaznu.edu.kz*

A.Z. Nurmukhanova *– Candidate of Technical Sciences, Associate Professor, Al-Farabi Kazakh National University, Almaty, Kazakhstan, e-mail: alfyia.nurmukhanova@kaznu.edu.kz*

A.A. Kuramay *– Master's student, Al-Farabi Kazakh National University, Almaty, Kazakhstan, e-mail: kuramaiabylai@gmail.com*

A.Zh. Balmaganbet *– Master's student, Al-Farabi Kazakh National University, Almaty, Kazakhstan, e-mail: balmaganbet2020@mail.ru*